Planta (1999) 210: 126–131

Planta

Heterogeneous inhibition of photosynthesis over the leaf surface of *Rosa rubiginosa* L. during water stress and abscisic acid treatment: induction of a metabolic component by limitation of CO_2 diffusion

Sylvie Meyer, Bernard Genty

Groupe Photosynthèse et Environnement, Laboratoire d'Ecophysiologie Végétale, Bât. 362, UPRESA 8079, Université Paris Sud, F-91405 Orsay, France

Received: 1 February 1999 / Accepted: 15 June 1999

Abstract. The contribution of changes in stomatal conductance and metabolism in determining heterogeneous photosynthesis inhibition during dehydration and abscisic acid (ABA) feeding was investigated using detached leaves of *Rosa rubiginosa* L. The steady-state and maximal rates of electron transport under a transient high CO_2 concentration were monitored using chlorophyll fluorescence imaging. The decrease in electron transport rate induced by dehydration and ABA treatment almost reverted to the control rate under transient high CO_2 availability. Therefore, inhibition of photosynthesis was mainly mediated through stomatal closure. However, since reversion was not complete, a metabolic inhibition was also identified as a decrease in the maximal electron transport rate driven by carboxylation. Under dehydration or ABA feeding, as under low ambient CO_2 treatment, in 21% or 0.4% O_2, the lower the steady-state electron transport was, the lower was the maximal electron transport rate during transient high CO_2 availability. We conclude that low CO_2 availability reduced the capacity of ribulose-1,5-bisphosphate carboxylase-oxygenase (Rubisco) to drive electron transport. The potential contribution of Rubisco deactivation mediated by stomatal closure is discussed.

Key words: Abscisic acid – Electron transport – *Rosa* (photosynthesis, stress) – Ribulose-1,5-bisphosphate carboxylase-oxygenase – Stomatal and metabolic inhibition – Water stress

Introduction

Photosynthesis can be heterogeneously distributed over a leaf, especially during periods of environmental stress. Though often related to heterogeneous stomatal closure (see Terashima et al. 1988; Terashima 1992), heterogeneity can also be due to heterogeneous metabolic activities (Bro et al. 1996). Thus, abscisic acid (ABA) treatment and water stress have been commonly reported to induce a stomatal closure and an often heterogeneous inhibition of leaf photosynthesis (Downton et al. 1988; Terashima et al. 1988; Wise et al. 1992). The lack of change in the photosynthetic capacity when measured by steady-state CO_2 or O_2 net exchanges under non-limiting CO_2 availability during ABA treatment or water stress (Terashima et al. 1988; Cornic et al. 1989; Graan and Boyer 1990) has been the main evidence for interpreting the inhibition as resulting purely from stomatal limitation of CO_2 diffusion (all studies but Graan and Boyer 1990).

However, this interpretation could be questioned since steady-state measurements under a high CO_2 concentration may alleviate a possible inhibition of photosynthetic metabolism if this inhibition depends on CO_2 availability (see e.g. Graan and Boyer 1990). Moreover, in vivo, the activation state of Rubisco has been reported to decrease when the intercellular CO_2 mole fraction (C_i) decreases (Perchorowicz and Jensen 1983; von Caemmerer and Edmonson 1986; Sage et al. 1990). Since there is evidence that under water stress (see Cornic and Massacci 1996) and ABA treatment (Lauer and Boyer 1992; Meyer and Genty 1998) photosynthesis operates under the low CO_2 availability which is the consequence of the stomatal closure, further work was needed to investigate the relationship between limitations on diffusion and changes in metabolic capacity.

In this study, by monitoring the maximal electron transport rate for CO_2 fixation under a transient high CO_2 concentration using chlorophyll fluorescence imaging, we analyse first the contribution of changes in stomatal conductance and metabolism in determining the heterogeneous inhibition of photosynthesis in

Abbreviations and symbols: ABA = abscisic acid; A_n = net rate of CO_2 assimilation; C_a = external CO_2 mole fraction; C_i = intercellular CO_2 mole fraction; g_s = stomatal conductance to H_2O; J_t = mean total electron transport rate; $(1 - \Phi/\Phi_m)$ = photochemical yield of PSII

Correspondence to: B. Genty;
E-mail: bernard.genty@eco.u-psud.fr; Fax: 33 (1) 69 15 72 38

detached leaves of *Rosa rubiginosa* L. dehydrated or fed with ABA. Then, we study the effect of restricted CO_2 availability on Rubisco activity in driving electron transport. We provide the first evidence that during dehydration, as during ABA treatment, a limitation of CO_2 availability mediated by stomatal closure can induce a reduction in the activation of Rubisco.

Materials and methods

Plant material. Plants were propagated from cuttings of *Rosa rubiginosa* L. collected on the campus (Orsay), and were grown in pots in a greenhouse under natural sunlight and photoperiod during summer, as described in Meyer and Genty (1998). Detached, fully expanded leaves were used with the petiole kept in distilled water throughout the experiment, as described in Bro et al. (1996).

Gas-exchange measurements. An open-flow gas-exchange system and a clamp-on leaf cuvette were used for the measurements of net CO_2 and water vapor exchanges as described in Meyer and Genty (1998). The cuvette temperature was kept constant at 25 °C. Gas-exchange parameters and leaflet temperature were calculated as described in Meyer and Genty (1998). Pulses of 0.74% v/v CO_2 in the cuvette with the leaf were obtained by injecting a given flow of pure CO_2 into the inlet of the humidified gas stream for approximatively 100 s. The concentration of CO_2 in the cuvette rose nearly instantaneously to a high level.

Mapping of PSII photochemical yield using chlorophyll fluorescence imaging and estimation of total photosynthetic electron transport rate. The method is described in detail in Genty and Meyer (1995). A video CCD camera (LHESA Electronique, Cergy Pontoise, France) imaged the chlorophyll fluorescence of the upper side of the leaflet surface from which gas-exchange measurements were performed. Routine cycles of two images, one of steady-state relative fluorescence yield, Φ, and the other of maximal relative fluorescence yield Φ_m were digitized and used to construct in near real time an image of the photochemical yield of PSII, $(1 - \Phi/\Phi_m)$, by computing pixel by pixel (Genty et al. 1989). Images of $(1 - \Phi/\Phi_m)$ and frequency-distribution histograms were computed as described in Meyer and Genty (1998). The mean total photosynthetic electron transport rate, J_t, was calculated from the mean $(1 - \Phi/\Phi_m)$ according to Genty et al. (1989; see also the legend of Table 1). Since images of $(1 - \Phi/\Phi_m)$ were obtained under constant irradiance, they can also be seen as maps of the relative rate of linear electron transport.

Protocol. Experiments were performed at a subsaturating photon flux density of 590–655 μmol m^{-2} s^{-1}. After a steady-state was reached in air, the leaf chamber CO_2 mole fraction (C_a) was lowered to 50 μmol CO_2 mol^{-1} for 1 h, raised again to normal mole fraction and subsequently varied in steps between ambient air composition and around 50 μmol CO_2 mol^{-1} and back to air composition. For dehydration treatment, the petiole was removed from water; for ABA treatment, *cis-trans* ABA (Sigma) was added to the water supply of the leaf petiole to bring its concentration to 10^{-4} M. Images of $(1 - \Phi/\Phi_m)$ were recorded just before and during a transition to 0.4% v/v O_2 for 3–5 min (i) before dehydration or ABA feeding, for normal and low C_a, and (ii) after dehydration or ABA feeding, when a pseudo-steady state was reached. Likewise, images of $(1 - \Phi/\Phi_m)$ were recorded in a 21 and 0.4% O_2 background during the transition pulse to 0.74% CO_2 30 s and 90 s after the start of the pulse. A subsaturating photon flux density was chosen so that a ribulose-bisphosphate-saturated condition was maintained for Rubisco activity at 340 μmol CO_2 mol^{-1} during the transition to 0.4% O_2 while keeping a large enough quantum yield of CO_2 assimilation for maximal accuracy of $(1 - \Phi/\Phi_m)$ imaging. At the end of the dehydration, the relative water content (RWC) was determined from a leaf disc (2.5 cm^2) as the ratio (fresh weight − dry weight)/(water-saturated weight − dry weight).

Table 1. Values of g_s, A_n, and J_t, for detached leaves of *Rosa rubiginosa* at steady-state photosynthesis before and during rapid dehydration and ABA feeding. Mean values and SD are given for five experiments for dehydration and three experiments for ABA treatment. During dehydrations the relative water content varied from 89.2 ± 3.1 to 68.5 ± 4.9%. Leaf atmosphere was about 330 μmol CO_2 mol^{-1}, 21% O_2 and 70% relative humidity. The photon flux density was 590–655 μmol m^{-2} s^{-1}. The mean total electron transport rate J_t was calculated according to $J_t = 4 \times [(1-\Phi/\Phi_m) - d] \times I/k$, where I is the incident photon flux density, k and d are the slope and the Y intercept of the linear relationship between mean $(1 - \Phi/\Phi_m)$ and the quantum yield of gross CO_2 assimilation obtained under non-photorespiratory conditions for each considered experiment (see Eq. 1 in Meyer and Genty 1998). For the experiments described here, k = 9.9 ± 1.1 (n = 8) and d = 0.037 ± 0.025 (n = 8)

	g_s (mmol m^{-2} s^{-1})	A_n (μmol m^{-2} s^{-1})	J_t (μmol m^{-2} s^{-1})
Rapid dehydration			
Control	302 ± 62	12.6 ± 1.8	103 ± 9
Dehydrated	37 ± 16	3.3 ± 1.4	73 ± 12
ABA treatment			
Control	313 ± 76	12.3 ± 2.1	97 ± 16
+ABA	50 ± 26	4.4 ± 1.0	71 ± 15

Results

Effects of dehydration and ABA feeding on gas exchanges and total electron transport rate. The kinetics of dehydration and ABA feeding effects on the net rate of CO_2 assimilation (A_n) and stomatal conductance to H_2O (g_s) were similar and like those described in a previous paper on ABA effects (Meyer and Genty 1998). Both A_n and g_s rapidly decreased about 20 min after the beginning of dehydration or ABA treatment and reached a new pseudo-steady state 40 min later. Both dehydration and ABA feeding induced a substantial decrease in A_n and g_s whereas J_t decreased less (70% of control value; Table 1), as commonly reported for dehydration (Cornic and Briantais 1991) and ABA treatment (Meyer and Genty 1998).

Heterogeneity of PSII photochemical yield and limitation of CO_2 diffusion. Figure 1 shows images of $(1 - \Phi/\Phi_m)$ and the corresponding frequency distributions for control and dehydrated leaves before (Fig. 1A,C) and during (Fig. 1B,D) a transition to 0.74% CO_2 in 0.4% O_2. In non-photorespiratory conditions (0.4% O_2), carboxylation of ribulose-1,5-bisphosphate is the only sink for electron transport; therefore, images of $(1 - \Phi/\Phi_m)$ were also images of the relative quantum yield of linear electron transport devoted to net CO_2 assimilation. During fast transition to 0.74% CO_2, images of $(1 - \Phi/\Phi_m)$ were images of the maximal rate of electron transport driven by carboxylation. The maximal rate of electron transport was reached 30 s after the start of the high-CO_2 transition in control and dehydrated leaves.

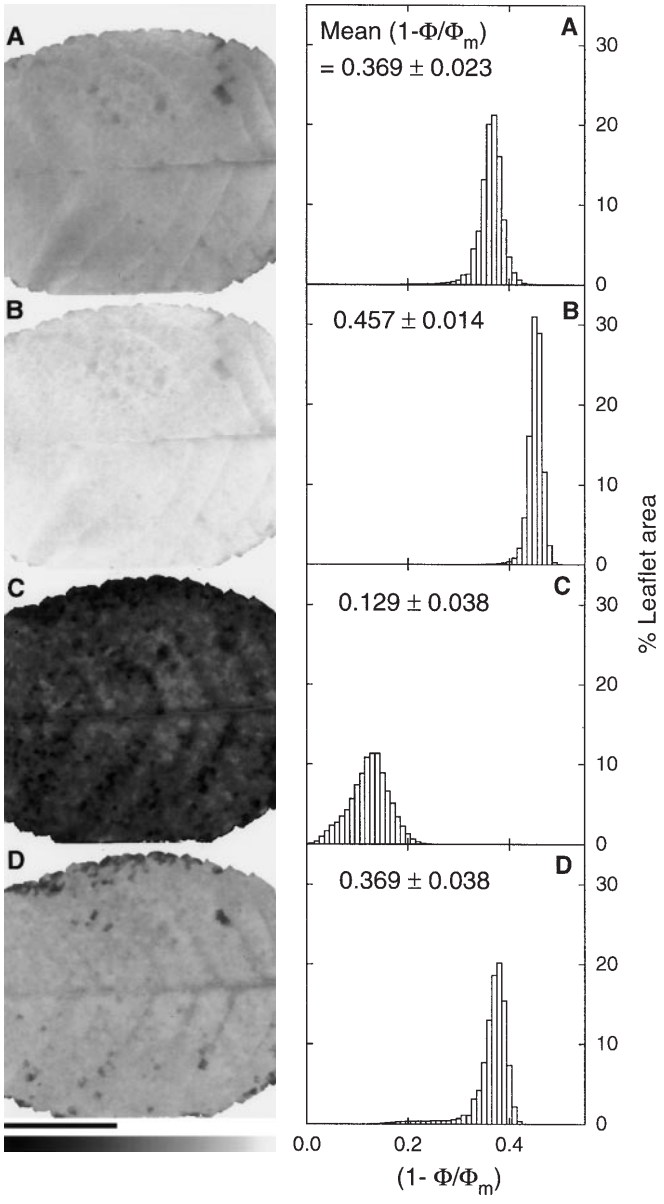

Fig. 1A–D. Images and frequency distributions of $(1 - \Phi/\Phi_m)$ taken during transition to 0.4% O_2 before (**A**,**C**) and 30 s after (**B**,**D**) the start of the transition to 0.74% CO_2 in control (**A**,**B**) and dehydrated (**C**,**D**) leaves of *Rosa rubiginosa* Ca was 310–340 μmol mol^{-1}. The photon flux density was 640 μmol m^{-2} s^{-1}. The bar indicates 1 cm. Three to four pixels correspond to the size of about one stoma and 10 epidermal cells. Pixel intensity was scaled using an eight-bit grey scale where black and white correspond to a photochemical yields of 0 and 0.5, respectively (**A**,**B**,**D**) or 0 and 0.4 respectively (**C**). The class size of the frequency distributions (expressed as a leaflet area percentage) was 0.01. Mean $(1 - \Phi/\Phi_m)$ ± SD are indicated. The g_s was 322 and 24 mmol m^{-2} s^{-1}, A_n was 22.8 and 3.1 μmol m^{-2} s^{-1} and C_i was 176 and 138 μmol mol^{-1} for **A** and **C**, respectively; J_t was 90, 113, 23 and 89 μmol m^{-2} s^{-1} for **A** through **D**, respectively

Before dehydration (Fig. 1A), at steady-state photosynthesis in 0.4% O_2, $(1 - \Phi/\Phi_m)$ was uniformly distributed over most of the leaflet area. The frequency distributions were unimodal and almost symmetrical. However, some sites (about 2% of the leaflet area) with a lower $(1 - \Phi/\Phi_m)$ appeared near the margins of the leaflet. In 21% O_2, these sites were not seen and $(1 - \Phi/\Phi_m)$ was always very uniform (data not shown, but see Bro et al. 1996; Meyer and Genty 1998). During brief exposure to high CO_2, $(1 - \Phi/\Phi_m)$ increased by about 25% over all the leaflet area (Fig. 1B) which showed that photosynthesis was not saturated at 340 μmol CO_2 mol^{-1}. The distribution of $(1 - \Phi/\Phi_m)$ also became much more uniform (Fig. 1B) showing that electron transport could be uniformly driven by CO_2 fixation over the leaflet area.

During dehydration, $(1 - \Phi/\Phi_m)$ heterogeneously decreased over the entire leaflet area according to a mosaic of small patches (Fig. 1C). The pattern of heterogeneity varied from experiment to experiment. However, the frequency distribution of $(1 - \Phi/\Phi_m)$ remained unimodal but with a larger coefficient of variation than the control and a substantial skew to the left. During a brief transition to 0.74% CO_2, the heterogeneity almost completely disappeared (Fig. 1D). The unimodal frequency distributions became narrower but remained slightly left-skewed because some sites on the leaflet, like the margins, presented low $(1 - \Phi/\Phi_m)$. Mean $(1 - \Phi/\Phi_m)$ reached a value between those obtained at normal and at high CO_2 concentrations in the control, showing that the maximal electron transport rate driven by carboxylation remained high after stomatal closure.

The rapidity and the extent of the reversion of mean $(1 - \Phi/\Phi_m)$ during transition to high CO_2 supply (Fig. 1C,D) show that dehydration mainly involved a heterogeneous limitation of CO_2 supply due to stomatal closure. This has already been described for ABA-fed leaves of *Rosa* in a previous paper (Meyer and Genty 1998). The lack of full recovery indicates that dehydration also induced a limitation of photosynthesis unrelated to CO_2 diffusion.

Changes in the maximal electron transport rate and its dependency on CO_2-diffusion-limited photosynthesis. To further analyze the inhibition of photosynthesis, we compared mean $(1 - \Phi/\Phi_m)$ obtained before and during transition to 0.74% CO_2 for control, dehydrated, and ABA-fed leaves in 0.4% O_2 (Fig. 2). The effect of CO_2 deficiency was also investigated by keeping the control leaf near the CO_2 compensation point in air for 1 h. At low CO_2 and O_2 concentrations, in contrast to control, dehydrated, and ABA-fed leaves, the maximal rate of electron transport driven by carboxylation was only reached 90 s after the start of the transition to high CO_2 (80% of the maximal value was obtained at 30 s). When the control leaf was kept in low CO_2 mole fraction (44 μmol CO_2 mol^{-1}), A_n, the mean $(1 - \Phi/\Phi_m)$ obtained before transition to 0.74% CO_2 and the mean $(1 - \Phi/\Phi_m)$ obtained 90 s after the start of this transition were lower by 80%, 66%, and 12–14%, respectively, compared to the control leaves. These decreases were similar to those induced by rapid dehydration (Fig. 2A) and larger than the decreases induced by ABA feeding (Fig. 2B). Whatever the treatment, the lower the mean $(1 - \Phi/\Phi_m)$ was before transition to 0.74% CO_2, the lower the mean $(1 - \Phi/\Phi_m)$ was during this transition.

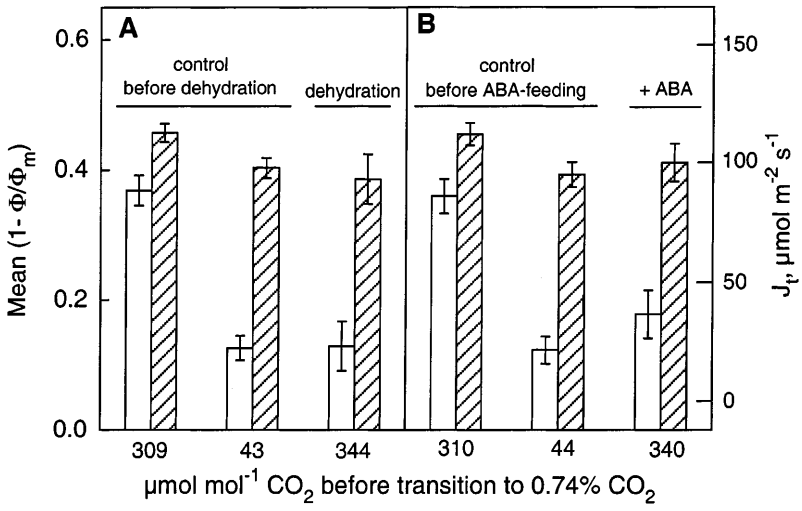

Fig. 2A,B. Changes in mean $(1 - \Phi/\Phi_m)$ obtained in 0.4% O_2 before (*open bars*) and during (*hatched bars*) transition to 0.74% CO_2. Mean $(1 - \Phi/\Phi_m)$ was estimated before and during dehydration (**A**; same leaf as in Fig. 1) or ABA feeding (**B**) in 309–344 µmol CO_2 mol^{-1} and also after keeping the control leaflet in 43–44 µmol CO_2 $mol^{-1}$for 1 h. During transition to 0.74% CO_2, mean $(1 - \Phi/\Phi_m)$ was obtained 30 s and 90 s after the start of the transition in 309–344 and 43–44 µmol CO_2 mol^{-1}, respectively. Error bars corresponded to the SD of mean $(1 - \Phi/\Phi_m)$. The corresponding mean J_t scale, computed from the equation given in the legend of Table 1 with k = 9.3 and d = 0.04, is shown on the *right axis*. Under 43–44 µmol CO_2 mol^{-1}, C_i was 24 and 28 µmol mol^{-1}, g_s was 366 and 459 mmol m^{-2} s^{-1}, and A_n was 3.7 µmol m^{-2} s^{-1} for **A** and **B**, respectively

This dependency was conserved for most sites of the leaflet (95% of the leaflet area) (data not shown).

The main point shown by Fig. 2 is that the maximal electron transport rate driven by carboxylation depended on the electron transport rate at steady-state photosynthesis estimated just before the transition to 0.74% CO_2. In addition, Fig. 3 shows that the dependency between mean $(1 - \Phi/\Phi_m)$ obtained during transition to 0.74% CO_2 and the mean $(1 - \Phi/\Phi_m)$ obtained before this transition followed a unique relationship whether the O_2 was 0.4 or 21% of the mixture before and during ABA feeding or low-CO_2 treatment. A similar dependency was obtained for dehydrated leaves (data not shown). For a given C_a, the mean $(1 - \Phi/\Phi_m)$ at steady-state photosynthesis was higher in 21% O_2 than in 0.4%

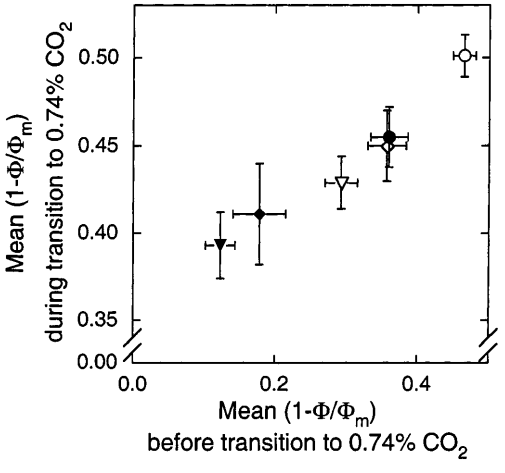

Fig. 3. Relationship between mean $(1 - \Phi/\Phi_m)$ obtained during transition to 0.74% CO_2 and mean $(1 - \Phi/\Phi_m)$ obtained before this transition. The oxygen mixing ratios were 21% O_2 (*open symbols*) and 0.4% O_2 (*closed symbols*). Mean $(1 - \Phi/\Phi_m)$ values of a control leaf held in 310–325 µmol CO_2 mol^{-1} (○, ●) or 1 h in 44–49 µmol CO_2 mol^{-1} (◇, ◆), and of an ABA-fed leaf (▽, ▼) in 335–340 µmol CO_2 mol^{-1} are shown. During the transition to 0.74% CO_2, mean $(1 - \Phi/\Phi_m)$ was obtained 30 s after the start of the transition except for the low-CO_2 treatment in 0.4% O_2, where it was obtained at 90 s. Error bars corresponded to the SD of mean $(1 - \Phi - \Phi_m)$

Table 2. Mean $(1 - \Phi/\Phi_m)$ obtained before and 30 s after the start of the transition to 0.74% CO_2 at steady-state photosynthesis for a *Rosa* leaflet held in 327 µmol CO_2 mol^{-1}, then in 49 µmol CO_2 mol^{-1} for 1 h and back to 327 µmol CO_2 mol^{-1}. The oxygen mixing ratio was 21%. Relative humidity and photon flux density were as described in Table 1. Each value is the mean of *n* experiments ± SD

	Mean $(1 - \Phi/\Phi_m)$ before transition to 0.74% CO_2	Mean $(1 - \Phi/\Phi_m)$ during transition to 0.74% CO_2
327 µmol CO_2 mol^{-1} (n = 7)	0.442 ± 0.026	0.486 ± 0.015
49 µmol CO_2 mol^{-1} for 1 h (n = 7)	0.254 ± 0.050	0.397 ± 0.029
Recovery in 327 µmol CO_2 mol^{-1} (n = 7, *n = 3)	0.434 ± 0.046	*0.484 ± 0.017

O_2 (Fig. 3) since O_2-dependent processes are a major sink for driving electron transport (see Meyer and Genty 1998). This unique relationship was always observed (eight experiments), whether the O_2 was present at 0.4 or 21%. This strongly suggests that the maximal electron transport rate driven by carboxylation depends on the total electron transport rate at steady-state photosynthesis but not on the partitioning of electron transport rate between carboxylation and oxygenation of ribulose-1,5-bisphosphate.

The decrease in mean $(1 - \Phi/\Phi_m)$ obtained before and during transition to 0.74% CO_2 after keeping the leaflet for 1 h near the CO_2 compensation point was fully reversed by reverting to the normal CO_2 concentration (Table 2). About 20 min was required for this reversion.

Discussion

In our study, the inhibition of photosynthesis after dehydration was mainly mediated through stomatal closure since the low electron transport rate almost

reversed to the control rate under transient high CO_2 availability. The rapidity and the extent of the reversion indicated that the metabolic capacity remained high during dehydration-induced inhibition of photosynthesis. The maintenance of a high electron transport rate in photorespiratory conditions during the course of the treatment was further evidence in favour of this interpretation. This confirms that limitation of CO_2 diffusion is the primary effect of short-term water stress (see Cornic and Massacci 1996). Therefore, the heterogeneity of photosynthesis induced by dehydration was caused by a heterogeneous distribution of stomatal closure over the leaflet area, as has been shown during ABA treatment (Meyer and Genty 1998). The frequency distributions of electron transport rate that were obtained over leaflets under non-photorespiratory conditions during dehydration and ABA feeding revealed unimodal distributions of stomatal conductance. Consequently, during dehydration the relative unresponsiveness of C_i in the presence of a limitation caused only by stomatal closure is unlikely to be exclusively due to non-uniform stomatal closure but also to appreciable cuticular transpiration, as has been shown for ABA treatment (Meyer and Genty 1998).

Our experiments also revealed a metabolic component that was identified as a decrease in maximal electron transport rate driven by carboxylation during transient saturating CO_2 availability. Similarities of the heterogeneous pattern of photosynthetic distribution before and during transient high CO_2 supply for dehydrated leaves (Fig. 1C,D) or ABA-fed leaves (data not shown) suggest that the spatial distribution of the diffusion-dependent limitation determined the spatial distribution of the metabolic inhibition. The metabolic inhibition of photosynthesis did not seem to directly result from dehydration, since low C_a, dehydration, and ABA-feeding treatments induced a comparable decrease in electron transport rate during transition to high CO_2 concentration (Figs. 2, 3). The low-C_a-induced decrease in maximal electron transport rate recovered fully under near-air CO_2 concentration with an estimated half-recovery time varying from 2 to 5 min. Therefore, this inhibition was likely to result from the decreased CO_2 availability during the stomatal closure induced by dehydration or ABA feeding. This provides further evidence that it was stomatal closure which primarily determined the inhibition of photosynthesis during dehydration and ABA feeding.

Interestingly, the partitioning of electron transport between ribulose-1,5-bisphosphate carboxylation and oxygenation during low-C_a, ABA feeding, and dehydration treatments did not modify significantly the dependency between the steady-state rate and the maximal rate of electron transport (Fig. 3): the lower the steady-state electron transport rate was, the lower the maximal electron transport rate driven by carboxylation was. This suggests that it is the steady-state electron transport rate more than the CO_2 availability that determines the maximal electron transport rate. Figure 4 shows that the maximal electron transport rate decreased when Rubisco activity limited the steady-state electron transport rate for C_i below 200 μmol mol^{-1}.

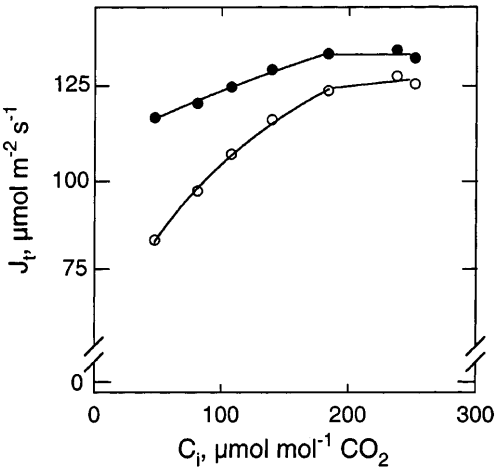

Fig. 4. Relationship of maximal and steady-state electron transport rates (J_t) versus intercellular CO_2 mole fraction (C_i) in a leaf of *Rosa* in 21% O_2. Maximal and steady-state values of J_t were determined before (○) and 30 s after (●) the start of the transition to 0.74% CO_2, respectively. The photon flux density was 640 μmol m^{-2} s^{-1}. The relationship was obtained by varying C_a. Fits were done as in Meyer and Genty (1998)

A change in Rubisco activation may explain this dependency. According to in vivo measurements giving a half-time of at least 2.5 min for Rubisco CO_2-dependent activation or deactivation (Perchorowicz and Jensen 1983), a 30-s duration between the start of the pulse of high CO_2 supply and the measurement of the maximal electron transport rate was expected not to be long enough to allow large changes in activation and catalytic activity of the enzyme. Consequently, the maximal electron transport rate driven by carboxylation measured during a pulse of high CO_2 concentration should be related to the Rubisco activation state at steady-state photosynthesis just before injection of a high CO_2 concentration. It is known that, in vivo, the activation state of Rubisco decreases when C_i decreases below 100 μmol CO_2 mol^{-1} under subsaturating irradiance (Perchorowicz and Jensen 1983; von Caemmerer and Edmonson 1986; Sage et al. 1990). Thus the treatments and low-CO_2-mediated inhibition of maximal electron transport rate reported here (Figs. 2, 4) were qualitatively consistent with the data and modeling of von Caemmerer and Edmonson (1986) and the data of Sage et al. (1990). However, under low CO_2 availability, it remains unknown whether Rubisco deactivation is a direct consequence of a deficiency in CO_2 activator used for enzyme carbamylation or a consequence of the reduction of steady-state electron transport rate used for activation. Our results suggests that a change in the steady-state electron transport rate mediated by stomatal closure may be a major component controlling the activation state of Rubisco in vivo.

In conclusion, the results presented here show that ABA feeding and dehydration mainly involved a limitation of CO_2 diffusion mediated by heterogeneous stomatal closure which in turn induced a non-uniformly

distributed reduction in Rubisco capacity. This metabolic inhibition is consistent with changes in enzyme activation, as has been previously shown under low C_a (Perchorowicz and Jensen 1983; von Caemmerer and Edmonson 1986; Sage et al. 1990). Our non-invasive approach using a CO_2 concentration jump which allows the diffusion limitation of photosynthesis to be removed and the maximal electron transport rate to be estimated should be a very powerful tool, allowing the relationship between the change in photosynthetic metabolism in vivo and CO_2 availability to be quantitatively described.

We thank F. Badeck (Institute for Climate Impact Research, Postdam, Germany) for helpful comments on the manuscript.

References

Bro E, Meyer S, Genty B (1996) Heterogeneity of leaf CO_2 assimilation during photosynthetic induction. Plant Cell Environ 19: 1349–1358; erratum Bro E, Meyer S, Genty B (1997) Plant Cell Environ 20: 275–276

Cornic G, Briantais JMB (1991) Partitioning of photosynthetic electron flow between CO_2 and O_2 reduction in a C3 leaf (*Phaseolus vulgaris* L.) at different CO_2 concentrations and during drought stress. Planta 183: 178–184

Cornic G, Massacci A (1996) Leaf photosynthesis under drought stress. In: Baker N (ed) Photosynthesis and the environment. Advances in photosynthesis, vol 5. Kluwer, Dordrecht, The Netherlands, pp 347–366

Cornic G, Le Gouallec JL, Briantais JM, Hodges M (1989) Effect of dehydration and high light on photosynthesis of two C_3 plants (*Phaseolus vulgaris* L. and *Elatostema repens* (Lour.) Hall f). Planta 177: 84–90

Downton WJS, Loveys BR, Grant WJR (1988) Non-uniform stomatal closure induced by water stress causes putative non-stomatal inhibition of photosynthesis. New Phytol 110: 503–509

Genty B, Meyer S (1995) Quantitative mapping of leaf photosynthesis using leaf chlorophyll fluorescence imaging. Aust J Plant Physiol 22: 277–284

Genty B, Briantais JM, Baker NR (1989) The relationship between the quantum yield of photosynthetic electron transport and quenching of chlorophyll fluorescence. Biochim Biophys Acta 990: 87–92

Graan T, Boyer JS (1990) Very high CO_2 partially restores photosynthesis in sunflowers at low water potentials. Planta 181: 378–384

Lauer MJ, Boyer JS (1992) Internal CO_2 measured directly in leaves. Abscisic acid and low leaf water potential cause opposing effects. Plant Physiol 98: 1310–1316

Meyer S, Genty B (1998) Mapping intercellular CO_2 mole fraction (C_i) in *Rosa rubiginosa* leaves fed with abscisic acid by using chlorophyll fluorescence imaging. Significance of C_i estimated from leaf gas exchange. Plant Physiol 116: 947–957

Perchorowicz JT, Jensen RG (1983) Photosynthesis and activation of ribulose bisphosphate carboxylase in wheat seedlings. Regulation by CO_2 and O_2. Plant Physiol 71: 955–960

Sage FR, Sharkey TD, Seemann JR (1990) Regulation of ribulose-1,5-bisphosphate carboxylase activity in response to light intensity and CO_2 in the C3 annuals *Chenopodium album* L. and *Phaseolus vulgaris* L. Plant Physiol 94: 1735–1742

Terashima I (1992) Anatomy of non-uniform leaf photosynthesis. Photosynth Res 31: 195–212

Terashima I, Wong SC, Osmond CB, Farquhar GD (1988) Characterisation of non-uniform photosynthesis induced by abscisic acid in leaves having different mesophyll anatomies. Plant Cell Physiol 29: 385–394

von Caemmerer S, Edmonson DL (1986) Relationship between steady-state gas exchange, in vivo ribulose bisphosphate carboxylase activity and some carbon reduction cycle intermediates in *Raphanus sativus*. Aust J Plant Physiol 13: 669–688

Wise RR, Ortiz-Lopez A, Ort DR (1992) Spatial distribution of photosynthesis during drought in field-grown and acclimated and non-acclimated growth chamber-grown cotton. Plant Physiol 100: 26–32